


Growth Dynamics of Crystalline Ar Hydrate

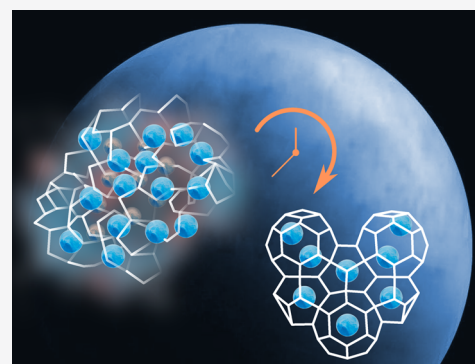
Samuele Fanetti, Demetrio Scelta, and Roberto Bini*

 Cite This: *J. Phys. Chem. C* 2020, 124, 10159–10166 Read Online

ACCESS |

 Metrics & More Article Recommendations

ABSTRACT: The formation of a clathrate hydrate crystal is characterized by several steps, each of them distinguished by a different structural arrangement and temporal duration. A precise definition of these different forms is a challenging task, because the entirety of the formation dynamics spans over a time interval ranging from few nanoseconds to several days. Computational methods are powerful and essential to define the nucleation step, but they fail in providing a reliable picture of the long-range order establishment. On the other side, the experimental methods employed in the study of the growth dynamics usually monitor the hydrate growth at the interface with the fluid and thus are limited by the diffusion of the guest molecules through the newly formed hydrate phase. This problem is overcome here by the confinement of an argon hydrate sample in a sapphire anvil cell, allowing monitoring of the melting and crystallization of hydrates under moderate pressures by FTIR and Raman spectroscopies. This approach, besides providing a spectroscopic characterization of this hydrate, allowed the time windows characteristic of the formation of a macroscopic amorphous phase to be identified, possibly coincident with the so-called *blob*, and its rapid evolution toward the achievement of the local structure. Long-range ordering takes place on a longer time scale, most of it is realized in few hours but still evolving for weeks. No hints for supporting the so-called *memory effect* are gained through this study.



1. INTRODUCTION

Clathrate hydrates are crystalline solids where polyhedral cages of hydrogen-bonded water molecules are stabilized by weak repulsive interactions between the guest molecules and the water molecules. Depending on the nature of the guest molecules, hydrogen bonding and other interactions can also be present, thus influencing structural and dynamical properties. Clathrate hydrates present three common structures: a primitive cubic *sI*, a face-centered *sII*, and a hexagonal *sH*.¹ The building block common to all the structures is the pentagonal dodecahedron (S^{12} cage), but due to the impossibility to fill the space with only this cage, polyhedrons possessing hexagonal faces are also required. The size of the guest molecules is important to define the cage type and hence the structure: smaller atoms or molecules, like some noble gases or the simplest diatomics, occupy smaller cages, so they preferentially form *sII* hydrates, which present the largest fraction of S^{12} cages.

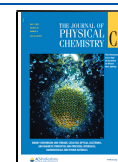
While the thermodynamics of hydrate formation/dissociation is well established, there are a lot of unanswered questions with respect to nucleation and growth. In the case of insoluble gases in water, the amount of guest molecules stored in these structures is even 3 orders of magnitude larger than that contained in the fluid phase from which it forms. For this reason, the homogeneous nucleation of the hydrate phase from the fluid mixture is very unlikely with respect to heterogeneous nucleation, which initiates at the interface between the water-

rich and the guest-rich phases. Once critical nuclei of the hydrate phase are formed (induction time), the hydrate growth takes place. Ripmeester and Alavi in their recent review² suggested that nucleation, decomposition, and the *memory effect* during reformation are among the most outstanding issues to be understood regarding clathrate hydrate science. Understanding hydrate nucleation at a molecular level is challenging due to the small time/length scales of nucleation and to the stochastic nature of the process. Both these aspects dramatically limit the experimental studies on the subject. The detectability of the process is intrinsically bound to the sensitivity of the chosen technique, as the early stages of nucleation may involve very few precursor species, which are also likely to be transient. The time (ps to hundreds of ns) and the length (nm) scales of the nucleation are not accessible by the usual experimental techniques employed for the characterization of the hydrates. Furthermore, nucleation is anticipated by an induction time necessary to reach the critical radii of the aggregates. The induction time is strictly related to oversaturation and metastability of the solution, and since

Received: January 15, 2020

Revised: April 2, 2020

Published: April 13, 2020



nucleation is a stochastic process, it is characterized by a significant scatter even in experiments performed under the same conditions.³ Because of all these difficulties in obtaining direct experimental evidence on this topic, hydrate nucleation has become a favorite subject for molecular simulation studies.^{4–9}

The differences among a variety of nucleation mechanisms, recently reviewed by Khurana et al.,³ are essentially related to the way in which the ordering of the water molecules is achieved and to the crystalline character of the clusters. Several reports support a faster ordering and then a faster nucleation when the fluid mixture is derived from hydrate-melt or ice-melt systems rather than from freshly prepared mixtures.^{1,10–12} Three main hypotheses have been formulated for explaining this issue, termed the *memory effect*, but no definitive indications allow their validity to be asserted.^{2,3} Among these three hypotheses, the one most subscribed to is that relating the faster nucleation to the presence of residual clusters of water molecules after the hydrate dissociation. Alternatively, a high local concentration of guest molecules or an active role of the impurities' surfaces in the decomposition and reformation cycle of the hydrates have been invoked as possible explanations of the observed reduction of the nucleation time of the hydrates. However, the validity of the *memory effect* is restricted to the vicinity of the melting conditions, vanishing the more and the longer the temperature is increased beyond the equilibrium conditions.^{11,12} Also, the crystalline or amorphous character of the nuclei and their temporal evolution is the subject of a lively debate mainly related to the way in which the water molecules are structured in the early nucleation stages.³ A multistep nucleation mechanism occurring through the formation of amorphous precursors and leading to the so-called *blob* formation was proposed by Jacobson et al.^{6,7} These amorphous precursors are guest-rich structures including also the same polyhedral cages as crystalline hydrates but lacking long-range order. The formation of amorphous nuclei was found to be kinetically favored with respect to the growth of crystalline nuclei but however led to the formation of crystalline clathrates.¹³

Experimental studies about the nucleation and growth of hydrates are mainly limited to pressures of the order of hundreds of bar or less, where the kinetics of the formation process is measured through the gas consumption rate, whereas higher-pressure studies are generally directed to the identification of crystal structures and phase boundaries. Diffraction and spectroscopic methods can be extremely useful to monitor *in situ* properties such as structure, cage occupancy, and composition without affecting the sample.^{14,15} Raman spectroscopy with high spatial resolution can be an excellent and versatile tool to monitor the sample homogeneity, whereas IR absorption spectroscopy, in view of its quantitative character, can serve to monitor the formation and growth kinetics of the hydrate in time scales longer than tens of seconds.

Among the variegated types of clathrate hydrates, the argon hydrate was the first noble gas hydrate to be discovered, and as for the hydrates of the heaviest elements of the same group, Xe and Kr, it is of great interest due to its supposed abundance on the surface of Titan.¹⁶ Also for this reason, Ar and Xe hydrates are the most studied noble gas hydrates under high-pressure conditions, where their structures have been characterized by synchrotron X-ray diffraction in combination with Raman spectroscopy¹⁷ or neutron diffraction.¹⁸ Here, we report a

study of the growth dynamics of argon hydrate crystals in a sapphire anvil cell (SAC) combining infrared absorption and Raman spectroscopy.

2. METHODS

Crystalline argon hydrate was prepared by means of a specifically designed high-pressure stainless steel vessel. This was filled with finely ground ice and cooled to 160 K with a mixture of solid and liquid ethanol, and then, it was sealed by using silver plated gaskets. The system was pumped for a couple of hours before argon was loaded while maintaining the vessel at 160 K. The argon pressure was raised up to 220 bar at this temperature. After about 30 min, the vessel is transferred to an ethyl glycol bath cooled at -33 °C using a chiller. The temperature was then increased in 3 h to -4 °C and then in 12 h to $+2$ °C where it was maintained for 6 h. The gas pressure increased up to 350 bar (-2 °C) to decrease to 200 bar after the cycle completion. The temperature was then lowered to -33 °C in the chiller, and then, the vessel was placed in liquid nitrogen where it was unsealed. The product appears as fine white flakes that are highly unstable at ambient temperature.

A membrane anvil cell equipped with sapphires having culets of 950 μm was employed for the high-pressure measurements. The sample was contained by a ~ 60 μm thick Cu–Be gasket drilled to a diameter of 450 μm . The loading of the sample was performed by quickly removing the hydrate crystals from the liquid nitrogen employed for their storage and placing them directly on top of the sapphires together with some ruby chips employed for the determination of the sample pressure by the ruby fluorescence method. For this operation, we placed the cell in a large vessel open only on the frontal side. Liquid nitrogen was used to keep the cell cold, and the amount of liquid nitrogen on the bottom of the vessel was such to have a large evaporation to ensure a dry atmosphere and avoid CO_2 contamination. In addition, we used a flux of dry nitrogen parallel to the open side to prevent contamination from the atmosphere. Once the sample was loaded, the cell was closed, and the membrane was pressurized. No CO_2 traces were detected in the sample by FTIR spectra. IR absorption spectra were measured using a Bruker IFS-120 HR Fourier transform IR spectrometer equipped with a globar lamp, KBr beam splitter, and MCT detector. An optical beam condenser based on ellipsoidal mirrors was used to focus the IR beam to a spot size comparable to the dimensions of the sample contained in the sapphire anvil cell.

Raman measurements were performed by using the 647.1 nm line of a Kr^+ laser as the excitation source. A backscattering geometry was adopted for the experiment using a long working distance $20\times$ Mitutoyo micro-objective. The spatial resolution on the sample is about 3 μm . Spectra are collected using a triple monochromator in subtractive dispersion mode (Acton/SpectraPro 2500i) equipped with holographic super notch filters and a CCD detector (Princeton Instruments Spec-10:100BR). The resolution used in both FTIR and Raman experiments is better than 1 cm^{-1} .

3. RESULTS

The structural evolution of Ar hydrate up to 1 GPa was characterized by neutron diffraction experiments.¹⁹ Up to 0.46 GPa, the stable structure is the typical cubic structure II of gas hydrates (CS-II) with a variable degree of filling of the large cavities increasing with rising pressure. Between 0.46 and 0.77

GPa, Ar hydrate has a hexagonal structure (HS-III) with up to five Ar atoms filling the large cavities. Above this pressure, up to 0.95 GPa, a new tetragonal structural type of gas hydrates containing only one type of polyhedral cavity with 14 faces is found (TS-IV); these polyhedrons are occupied by two argon atoms each. The stability at higher pressures of Ar hydrate has been proven by different studies.^{18,20–22} Visual observation and Raman spectra were employed to determine the decomposition curve of the hydrate up to 3 GPa.²⁰ Two other quadruple points were identified in the same study for pressures in excess of 1 GPa, but only one clathrate hydrate structure is reported. A very dense structure was suggested for this phase according to the steep slope of the decomposition curve,²¹ and successive X-ray diffraction studies²² identified this high-pressure phase as a body-centered orthorhombic structure closely recalling the filled ice structure.²³ According to the available data,^{19,20} the melting of argon hydrate below 2 GPa shows a demixing of the fluid phase with a water-rich liquid phase and an Ar-rich fluid phase.²⁰ In addition, a strong metastability of the fluid mixture is observed when the temperature is isobarically reduced for inducing the hydrate recrystallization. Above 0.5 GPa, the clathrate formation is achieved only when the fluid is cooled down until the obtainment of the corresponding ice phase with the clathrate forming at the ice-liquid interface.²⁰

In this study, we used Raman and infrared absorption spectroscopies to monitor the growth kinetics of Ar hydrate from the fluid phase to understand the structural evolution of the hydrate along the different steps of the crystallization process. Once the loading of the Ar hydrate crystals was completed, we brought the cell to ambient temperature, and the sample pressure was adjusted to 0.6 GPa. At these pressure–temperature (P – T) conditions, the argon hydrate is in the HS-III phase¹⁹ whereas no water ice should be present being well inside the liquid stability region. Visual inspection of the sample reveals an appearance consistent with a homogeneous polycrystal. In Figure 1, we report the Raman spectrum measured at these P – T conditions in the lattice phonon region. The spectrum, to our knowledge reported here for the first time, is very similar to that of Xe hydrate measured at ambient pressure and low temperature.²⁴ The most intense band is by far the one at 227 cm^{-1} , which also closely resembles that observed in ice and for this reason is associated with deformation modes of the water molecules.²⁵ The similarities with the Xe hydrate spectrum extends also at lower frequencies, where at least four other bands, at 35, 56, 80, and 132 cm^{-1} , with a similar relative intensity distribution are observed, although the Xe hydrate frequencies are systematically lower. These bands must be related to translational modes in analogy with the case of ice, whose II, V, and VI crystals underlay the high-pressure hydrate structures.

The temperature was then raised in steps of 0.1 K while the sample was observed under the microscope. Melting was observed at 306.9 K (0.61 GPa) by the formation of small bubbles, likely composed by Ar. A Raman mesh of the sample collected at this stage shows in every point the typical spectrum of a liquid (red trace in Figure 1), thus confirming the melting occurrence. The P – T conditions for the melting are in perfect agreement with the decomposition line of ref 19. The temperature was then lowered again while the sample was monitored by microscope. At 298 K, the sample abruptly becomes homogeneous with the disappearance of the Ar

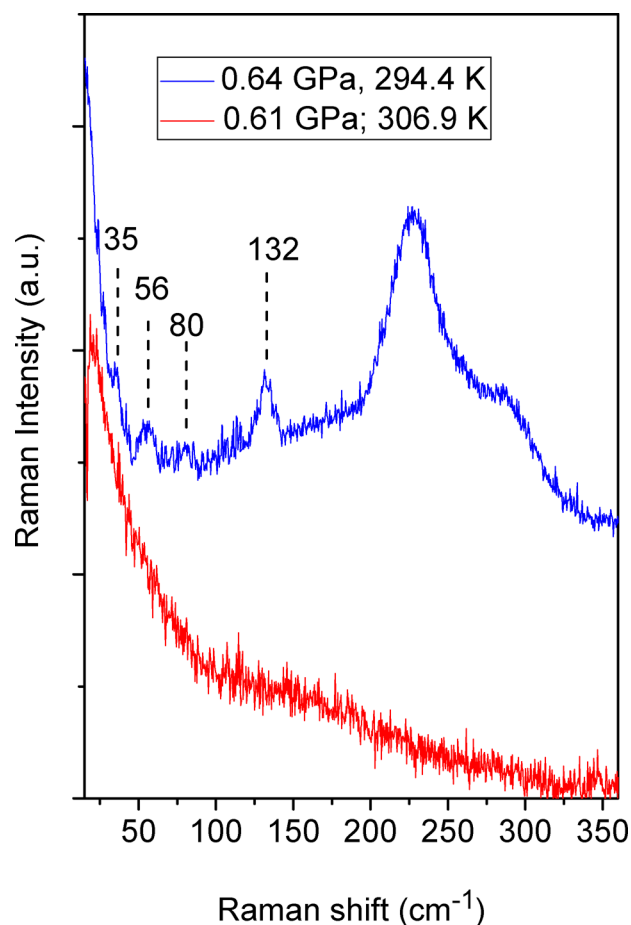


Figure 1. Raman spectrum collected in the low-frequency region before melting of Ar hydrate (blue trace, 0.64 GPa; 294.4 K) and in molten sample (red trace, 0.61 GPa; 306.9 K). The low-frequency lattice modes are indicated in the crystal spectrum by dashed ticks, and the relative frequency values are also indicated.

bubbles; however, the Raman spectrum collected immediately after this sudden change was noticed does not show any remarkable difference with respect to the fluid (black trace in Figure 2). The spectrum slowly evolves in time while maintaining an unchanged P and T , and after 1.5 h, the strongest band of the hydrate crystal at 227 cm^{-1} starts to be visible. The progressive formation of all the spectral signatures of the hydrate crystal takes place in about 3 h. This behavior is better evidenced in the bottom panel of Figure 2, where the area of the band at 227 cm^{-1} is reported as a function of time. After this initial stage, the sample keeps changing with time, and Raman mapping evidences a water-rich area in the center of the sample, which progressively reduces, disappearing after several days when a perfectly homogeneous crystalline sample is obtained.

We melted again the hydrate crystal under the microscope, to better characterize the hydrate crystallization, observing the decomposition at 305 K (0.66 GPa). The molten sample was left at 300 K and 0.66 GPa for about 4 days (90 h) without any change in the sample appearance being observed. Consistently, the Raman spectrum was always that of a liquid phase. FTIR spectroscopy was then employed to monitor the crystallization kinetics. The sample was cooled in steps of 1 K while its evolution was continuously monitored by measuring the IR spectrum. Crystallization was observed at 295 K (0.66 GPa) by

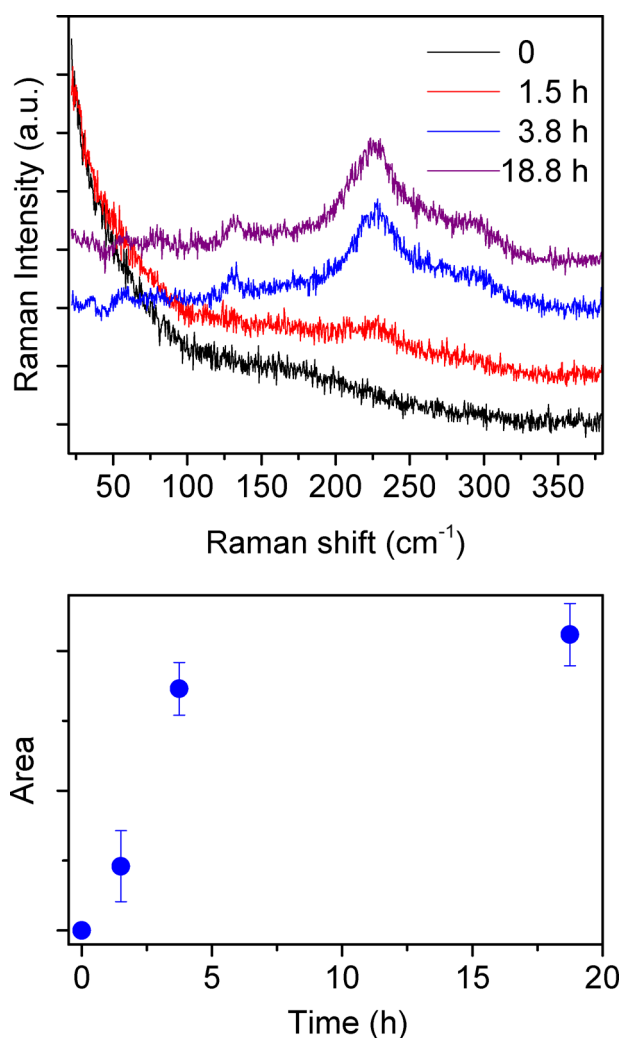


Figure 2. Top: Raman spectra measured in the lattice phonons region during the crystallization process at 298 K and 0.61 GPa. Bottom: Evolution with time of the intensity of the Raman band at 227 cm⁻¹.

the sudden change of the transmission through the sample of a probe laser beam and, at the same time, of the interferogram's center peak amplitude. Infrared spectra have been collected from this moment, assumed as the beginning of the crystallization, at time intervals varying from 5 min (initial stages) to 30 min. Pressure was monitored every few minutes during the first step of the crystallization, and it was found to be constant within the accuracy of its determination (± 0.01 GPa). Some of the IR absorption spectra are shown in Figure 3 in the region of a combination band of water, bending plus H-bond libration ($\nu_2 + L$), which is used as a probe of the transition as it is always in scale and changes considerably upon crystallization. The same behavior is also observed in pure ice, where a shift of about 70 cm⁻¹ is measured (from 2150 to 2220 cm⁻¹) at ambient pressure.²⁶

The spectra have been reproduced with three Gaussian profiles (see Figure 4) at the initial stages of the crystallization process ($t \leq 3$ h), the lowest peak being related to liquid water and the other two higher-frequency peaks being related to the hydrate. The frequency and width of the liquid band were fixed to the values measured in the molten hydrate before crystallization, and only its intensity was left changing. This band vanishes in about 1.5 h. The fit parameters of the two

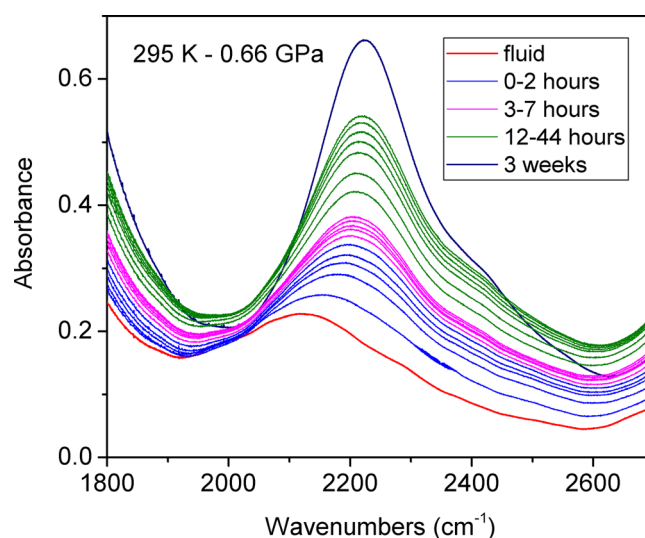


Figure 3. Time evolution of the infrared absorption spectrum in the region of the bending plus H-bond libration ($\nu_2 + L$) combination band of water. In the plot are reported only a few selected spectra grouped on the basis of their temporal separation: the red trace is the last spectrum acquired in the fluid; blue traces are those collected at the beginning of the crystallization process and are separated by 0.5 h; the magenta traces are separated by 1 h, whereas the green traces are separated by 5 h. The time intervals covered in the three cases are indicated in the legend. The last trace is relative to the hydrate after 3 weeks.

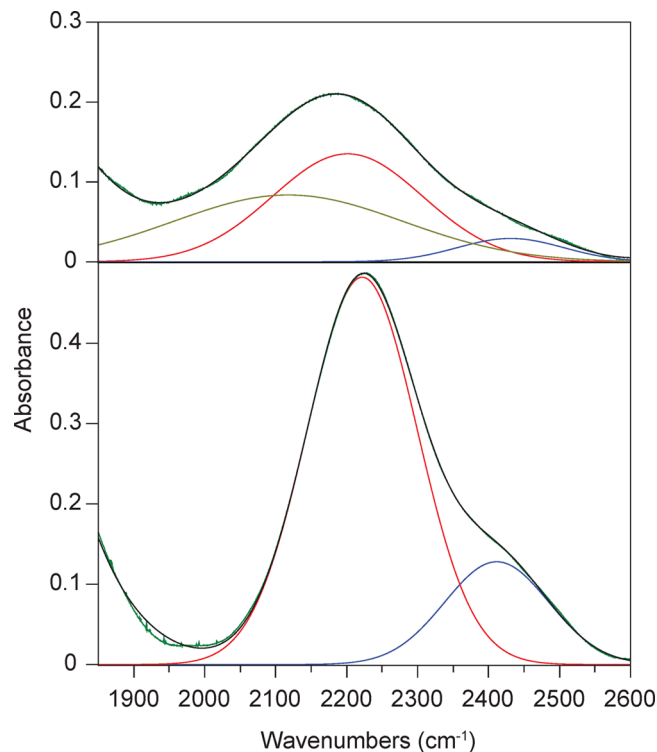


Figure 4. Representative deconvolution results of the $\nu_2 + L$ combination band of Ar hydrate. Top: Deconvolution of the spectrum acquired 1 h after the beginning of the crystallization; the three Gaussian bands employed in the fit are relative to liquid water (lowest-frequency band, dark yellow) and to the hydrate (red and blue). Bottom: Deconvolution of the spectrum acquired after 3 weeks; only two Gaussian bands are used, since the sample is entirely crystalline.

hydrate bands (peak frequency, fwhm, and area) and the area of the liquid band are reported as a function of time in Figures 5 and 6. The most intense peak (labeled as peak 1) is initially

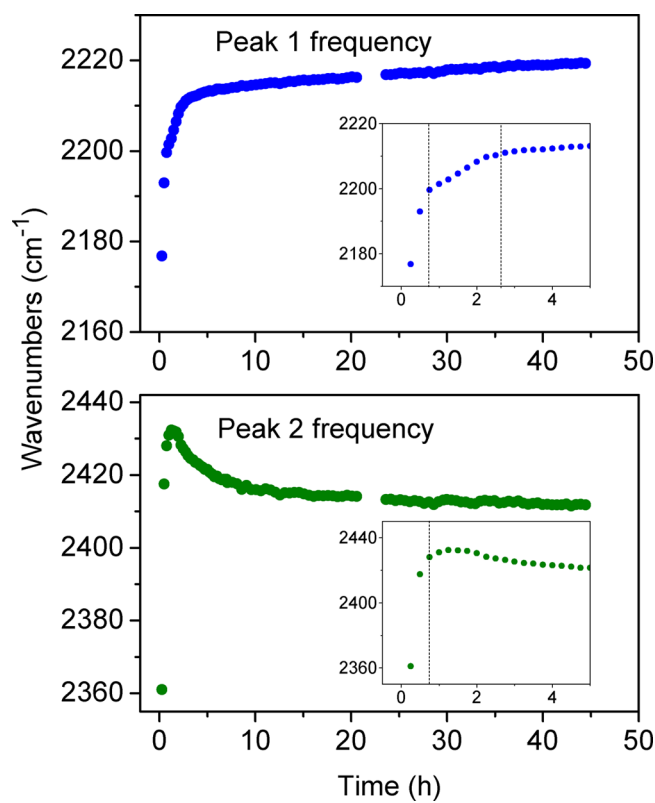


Figure 5. Time evolution of the peak frequencies of the two Gaussian bands employed to reproduce the bending plus H-bond libration combination band of water after the crystallization started at 0.66 GPa and 295 K. In the insets, the details of the first 5 h of the kinetics are reported. The dashed lines are eye guides to identify the time intervals characterized by a similar rate of the frequency change.

just above 2170 cm^{-1} , rapidly shifting to the blue by more than 40 cm^{-1} , the second (peak 2), much weaker and clearly visible only at longer delays, is initially at 2360 cm^{-1} , also undergoing a 70 cm^{-1} blue shift with time. In spite of some differences in the time evolution of the two peaks, such as the opposite sign of the frequency shift once the faster steps of the crystallization are terminated (see Figure 5 for $t \leq 2\text{ h}$), the two bands behave in a similar way in all the time ranges investigated, being therefore related to the hydrate formation.

The time evolution of the frequencies and fwhm highlights a formation dynamics of the hydrate composed by two distinct regimes. The first one, evidenced in the insets of Figure 5, characterizes the first 0.5 h, where a huge change of the peak frequency is accompanied by an equally fast line narrowing and intensification (see Figure 6). This evolution slows down in the following 2 h while a remarkable rate, especially as the fwhm is concerned, is maintained. This behavior closely recalls the intensification of the hydrate lattice phonons measured by Raman (see Figure 2), which also takes place in the first 3 h. After these rapid steps, there is a much slower evolution of all the parameters that monotonically evolve over a time interval of about 2 days. In this second regime, the peak frequencies are not much affected, changing by about 1%; on the contrary, the integrated area and the peak 1 line width remarkably increases by 60% and reduces by 20%, respectively.

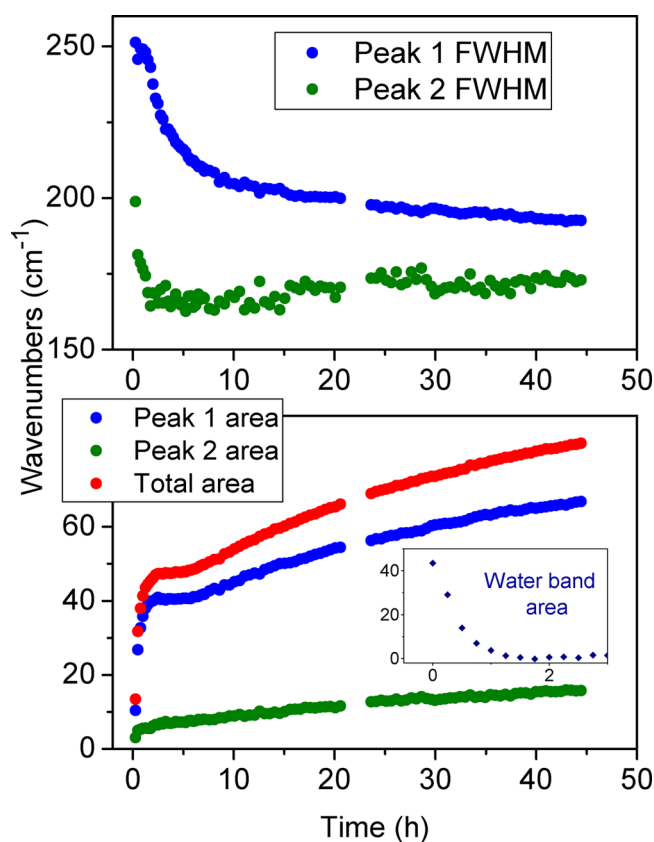


Figure 6. Time evolution of the full width at half-maximum (fwhm) and area of the two Gaussian bands employed to reproduce the bending plus H-bond libration combination band of water in the hydrate after the crystallization started at 0.66 GPa and 295 K. In the lower panel, the inset reports the time evolution of the area of the band relative to liquid water.

4. DISCUSSION

The nucleation of a gas hydrate crystal has been identified as a two-step process characterized by the fast (ns to μs) formation of disordered solid-like structures evolving on much longer time scales toward crystalline forms.²⁷

The first-stage state is difficult to be recognized, at least experimentally, being characterized by short-range ordering with a local structure and energy reflecting those of a crystal. A two-step mechanism was independently identified in different computational studies of systems like methane,²⁷ H_2S ,²⁸ and CO_2 ,²⁹ with the rate of the first step depending critically on the concentration of guest molecules, speeding up with an increase of the supersaturation conditions of guest species. This two-step mechanism is further detailed by Jacobson et al.,⁶ where the first step is divided into two phases characterized by *blob* and amorphous structures. The two species differ for the water molecules' arrangement in hydrogen-bonded polyhedral cages, which are not yet present in the *blob* and achieved only in the amorphous phase. This two-stage mechanism should not be confused with the one identified in several experimental studies of hydrate formation at large interfaces, which is the most characteristic condition where hydrates are experimentally studied. In these cases in fact, the fast process, coating of the ice surface, takes from seconds to minutes followed by a much slower growth related to the diffusion of host species through the hydrates to reach the reaction sites. For example, in the X-ray microtomography study of Xe hydrate formation at the

Xe–ice interface, the initial quasi-two-dimensional growth along the ice surface occurs in a few minutes to extend, at later stages, toward the gas phase and inside the ice, resulting in the appearance of lens-shaped Xe hydrate crystals after about 10 h.³⁰ NMR spectroscopy was also employed to monitor the nucleation and growth of Xe hydrate on the ice surface, succeeding in measuring the first minutes of the hydrate formation.³¹ After this time window, corresponding to the establishment of hydrate layers tens of nanometers thick, the reaction became extremely slow. Very similar time windows were also found in combined Raman and X-ray diffraction study of CO₂ hydrate formation.³² The explanation of this slowdown should be searched in the diffusion of the guest molecules through the hydrate, which limits the crystal growth propagation.

In the present case, the Ar hydrate formation occurs from a mixture where the Ar-rich fluid phase is finely dispersed in the water-rich liquid phase, making the interface between the two phases extremely large. This arrangement should allow the observation of the full growth dynamics of the hydrate. Even after a few days, in which this mixture was left to equilibrate, we did not observe any appreciable change in the sample aspect. The clathrate always formed from slightly supercooling the fluid; indeed, crystallization is always observed to take place between 300 and 290 K at pressures ranging between 0.6 and 0.7 GPa. This observation disagrees with the report by Lotz et al.,²⁰ which at similar pressures and in very similar environmental conditions, since they also conducted experiments in DAC, succeeded in the crystallization, only with a more pronounced supercooling, observing first the crystallization of ice phases and only successively the clathrate formation. This difference could be ascribed to the fact that their samples were prepared with a large excess of water. In our experiments, we could not also recognize any relation between the time elapsed from the establishment of the crystallization conditions and its occurrence, the amount of time the sample was left in the fluid phase and of the thermal treatment to which it was subjected. In other words, we have no hints of a possible *memory effect*. However, although the time scale where we can probe this event is orders of magnitude longer than the characteristic nucleation times, other experiments on the formation of Xe hydrate, conducted with a time resolution comparable to ours, observed a decrease of the induction time with increasing the Xe gas pressure, vanishing when the hydrate was pumped to remove the Xe and then re-exposed to the gas.³¹ The latter issue was taken as an indication of a kind of “preorganization” of the surface for hydrate growth. Nevertheless, statistical studies of hydrate nucleation based on visual observations in a system subjected to formation/dissociation cycles showed the complete stochastic nature of this event, evidencing an important role of the thermal history.³³ A *memory effect* of the water molecules governing the nucleation process was also invoked in energy dispersive X-ray diffraction measurements to explain the extreme variability of the nucleation time of CO₂ hydrates depending on the way water was prepared.¹¹ However, neutron diffraction studies of methane hydrate formation and decomposition did not evidence any change in the coordination number of water molecules around methane (water structure) before the hydrate growth and after the hydrate decomposition.³⁴

The kinetics of the hydrate formation measured in this work by FTIR spectroscopy clearly evidence two temporally distinct steps. The first one approximately covers the first 30 min and is

characterized by a steep increase of the peak frequency value (30–70 cm⁻¹) of both components of the $\nu_2 + L$ combination band of water. The frequency of the main band still increases in the successive 1.5–2.0 h but at a considerably smaller rate, about 10 cm⁻¹ h⁻¹. This time window nicely agrees also with the Raman data, which show the appearance from the liquid-like spectrum of the lattice phonon bands after about 1 h, to evolve rapidly in the successive 2–3 h. For longer delays, the evolution of the two IR peaks is very similar being characterized by a continuous smooth variation of the frequency, although the most intense peak still blue shifts, whereas the weaker peak moves back to lower frequencies. A very similar behavior is also shown by the fwhm and the area of the two peaks, which exhibit a remarkable narrowing and intensification in the first half hour, to smoothly decrease the rate change for longer delays. The time evolution of these parameters provides a considerable insight about the hydrate structural changes at the microscopic level. The vibrational frequency in a molecular crystal is indeed an efficient probe of the local environment, whose changes can produce frequency shifts of the order of some percent. In this case, the mode under examination is extremely sensitive to the crystallization as also observed in pure water.²⁶ As already mentioned, this mode is a combination of the bending and of the H-bond libration, and the large frequency shift occurring at the melting is ascribable to the libration, which, upon crystallization, undergoes in pure water a blue shift comparable to that of the combination mode.³⁵ However, the crystallization process, which in ice takes place on a shorter time scale (μs to ms ³⁶), lasts in this case several minutes, attesting for complex dynamics likely related to the construction of the local environment, *i.e.*, the hydrate cage. The evolution of the fwhm spans instead over a much larger time interval, showing an appreciable narrowing even after several hours. This parameter is related to the relaxation dynamics, which rule the lifetime of the state, and it is an efficient probe of the translational order. We therefore expect an evolution for this parameter approximately mirroring the evolution of the lattice phonon spectra being both related to the long-range order building in the crystal.

5. CONCLUSIONS

The confinement of crystalline Ar hydrate in a sapphire anvil cell allowed us to carefully monitor by spectroscopic methods the melting and the following recrystallization process. We have neither any indication of a possible existence of a *memory effect* nor excessive supercooling of the sample to induce crystallization. The molten mixture is composed by finely dispersed Ar microbubbles, thus ensuring a huge surface contact between water-rich and Ar-rich phases. The transition to the solid phase is visually and optically detected and confirmed by IR absorption spectra in the region of the $\nu_2 + L$ combination band of water. The crystal formation is characterized by different steps that we are able to characterize, starting from the growth of the existing amorphous nuclei until the achievement of high-quality macroscopic crystals. These steps are identified through the variation of the spectral parameters of the $\nu_2 + L$ band and by the Raman spectrum of the lattice phonons, reported here for the first time. An amorphous structure is built on a time scale not accessible in our experiments. The local rearrangement, which we can monitor through the frequency change of the $\nu_2 + L$ band, is very important in the first half hour time window, where, on

the other side, a long-range order (lattice phonons) is not yet established. In the following 1–1.5 h, the local structure is realized, and we have evidence of the establishment of long-range order (translational symmetry) of the hydrate. Although the rate of this last process tends to stabilize after 10 h, with most of the long-range ordering being realized within this time interval, the hydrate evolution keeps going on for several days.

AUTHOR INFORMATION

Corresponding Author

Roberto Bini – Dipartimento di Chimica “Ugo Schiff”,
Università di Firenze, I-50019 Firenze, Italy; LENS, European
Laboratory for Non-linear Spectroscopy, I-50019 Firenze, Italy;
ICCOM-CNR, Istituto di Chimica dei Composti
OrganoMetallici - Consiglio Nazionale delle Ricerche, I-50019
Firenze, Italy; orcid.org/0000-0002-6746-696X;
Email: roberto.bini@unifi.it

Authors

Samuele Fanetti – ICCOM-CNR, Istituto di Chimica dei
Composti OrganoMetallici - Consiglio Nazionale delle Ricerche,
I-50019 Firenze, Italy; LENS, European Laboratory for Non-
linear Spectroscopy, I-50019 Firenze, Italy; orcid.org/0000-0002-5688-6272

Demetrio Scelta – ICCOM-CNR, Istituto di Chimica dei
Composti OrganoMetallici - Consiglio Nazionale delle Ricerche,
I-50019 Firenze, Italy; LENS, European Laboratory for Non-
linear Spectroscopy, I-50019 Firenze, Italy; orcid.org/0000-0002-4856-0125

Complete contact information is available at:
<https://pubs.acs.org/10.1021/acs.jpcc.0c00386>

Notes

The authors declare no competing financial interest.

ACKNOWLEDGMENTS

We thank the European Laboratory for Nonlinear Spectroscopy (LENS) for hosting the research, the Deep Carbon Observatory, and the Fondazione CR Firenze for strong support. The research has been supported by the following grants: “Extreme Physics and Chemistry of Carbon: Forms, Transformations, and Movements in Planetary Interiors” funded by the Alfred P. Sloan Foundation; “DReaMS UP - Dynamics of Reactivity in Molecular Systems Under Pressure”; Fondazione Cassa di Risparmio di Firenze under the projects “Dinamiche di fusione di ghiacci e idrati: accesso al regime mesoscopico” and “HP-PHOTO-CHEM”. We also thank MIUR-Italy (“Progetto Dipartimenti di Eccellenza 2018-2022” allocated to Department of Chemistry “Ugo Schiff”).

REFERENCES

- (1) Sloan, Jr., E. D.; Koh, C. A. *Clathrate Hydrates of Natural Gases*, 3rd ed.; CRC Press: Boca Raton, FL, 2007.
- (2) Ripmeester, J. A.; Alavi, S. Some Current Challenges in Clathrate Hydrate Science: Nucleation, Decomposition and the Memory Effect. *Curr. Opin. Solid State Mater. Sci.* **2016**, *20*, 344–351.
- (3) Khurana, M.; Yin, Z.; Linga, P. A Review of Clathrate Hydrate Nucleation. *ACS Sustainable Chem. Eng.* **2017**, *5*, 11176–11203.
- (4) Moon, C.; Taylor, P. C.; Rodger, P. M. Molecular Dynamics Study of Gas Hydrate Formation. *J. Am. Chem. Soc.* **2003**, *125*, 4706–4707.
- (5) Walsh, M. R.; Koh, C. A.; Sloan, E. D.; Sum, A. K.; Wu, D. T. Microsecond Simulations of Spontaneous Methane Hydrate Nucleation and Growth. *Science* **2009**, *326*, 1095–1098.

(6) Jacobson, L. C.; Hujo, W.; Molinero, V. Amorphous Precursors in the Nucleation of Clathrate Hydrates. *J. Am. Chem. Soc.* **2010**, *132*, 11806–11811.

(7) Jacobson, L. C.; Hujo, W.; Molinero, V. Nucleation Pathways of Clathrate Hydrates: Effect of Guest Size and Solubility. *J. Phys. Chem. B* **2010**, *114*, 13796–13807.

(8) Sarupria, S.; Debenedetti, P. G. Homogeneous Nucleation of Methane Hydrate in Microsecond Molecular Dynamics Simulations. *J. Phys. Chem. Lett.* **2012**, *3*, 2942–2947.

(9) Knott, B. C.; Molinero, V.; Doherty, M. F.; Peters, B. Homogeneous Nucleation of Methane Hydrates: Unrealistic under Realistic Conditions. *J. Am. Chem. Soc.* **2012**, *134*, 19544–19547.

(10) Parent, J.; Bishnoi, P. Investigations into the Nucleation Behaviour of Methane Gas Hydrates. *Chem. Eng. Commun.* **1996**, *144*, 51–64.

(11) Takeya, S.; Hori, A.; Hondoh, T.; Uchida, T. Freezing-Memory Effect of Water on Nucleation of CO₂ Hydrate Crystals. *J. Phys. Chem. B* **2000**, *104*, 4164–4168.

(12) Sefidroodi, H.; Abrahamsen, E.; Kelland, M. A. Investigation into the Strength and Source of the Memory Effect for Cyclopentane Hydrate. *Chem. Eng. Sci.* **2013**, *87*, 133–140.

(13) Jacobson, L. C.; Molinero, V. Can Amorphous Nuclei Grow Crystalline Clathrates? The Size and Crystallinity of Critical Clathrate Nuclei. *J. Am. Chem. Soc.* **2011**, *133*, 6458–6463.

(14) Murshed, M. M.; Kuhs, W. F. Kinetic Studies of Methane-Ethane Mixed Gas Hydrates by Neutron Diffraction and Raman Spectroscopy. *J. Phys. Chem. B* **2009**, *113*, 5172–5180.

(15) Ohno, H.; Strobel, T. A.; Dec, S. F.; Sloan, E. D., Jr.; Koh, C. A. Raman Studies of Methane-Ethane Hydrate Metastability. *J. Phys. Chem. A* **2009**, *113*, 1711–1716.

(16) Thomas, C.; Mousis, O.; Ballenegger, V.; Picaud, S. Clathrate Hydrates as a Sink of Noble Gases in Titan’s Atmosphere. *Astron. Astrophys.* **2007**, *474*, L17–L20.

(17) Sanloup, C.; Mao, H. K.; Hemley, R. J. High-Pressure Transformations in Xenon Hydrates. *Proc. Natl. Acad. Sci. U. S. A.* **2002**, *99*, 25–28.

(18) Loveday, J. S.; Nelmes, R. J.; Klug, D. D.; Tse, J. S.; Desgreniers, S. Structural Systematics in the Clathrate Hydrates Under Pressure. *Can. J. Phys.* **2003**, *81*, 539–544.

(19) Manakov, A. Y.; Voronin, V. I.; Kurnosov, A. V.; Teplykh, A. E.; Komarov, V. Y.; Dyadin, Y. A. Structural Investigations of Argon Hydrates at Pressures up to 10 Kbar. *J. Inclusion Phenom. Mol. Recognit. Chem.* **2004**, *48*, 11–18.

(20) Lotz, H. T.; Schouten, J. A. Clathrate Hydrates in the System H₂O-Ar at Pressures and Temperatures up to 30 kbar and 140 °C. *J. Chem. Phys.* **1999**, *111*, 10242.

(21) Dyadin, Y. A.; Larionov, E. G.; Mirinski, D. S.; Mikina, T. V.; Starostina, L. I. Clathrate Formation in the Ar-H₂O System Under Pressures up to 15000 bar. *Mendeleev Commun.* **1997**, *7*, 32–33.

(22) Hirai, H.; Uchihara, Y.; Kawamura, T.; Yamamoto, Y.; Yagi, T. Pressure-Induced Phase Changes of Argon Hydrate and Methane Hydrate at Room Temperature. *Proc. Jpn. Acad., Ser. B* **2002**, *78*, 39–44.

(23) Loveday, J. S.; Nelmes, R. J.; Guthrie, M.; Klug, D. D.; Tse, J. S. Transition from Cage Clathrate to Filled Ice: The Structure of Methane Hydrate III. *Phys. Rev. Lett.* **2001**, *87*, 215501.

(24) Adichtchev, S. V.; Belosludov, V. R.; Ildyakov, A. V.; Malinovsky, V. K.; Manakov, A. Yu.; Subbotin, O. S.; Surovtsev, N. V. Low-Frequency Raman Scattering in a Xe Hydrate. *J. Phys. Chem. B* **2013**, *117*, 10686–10690.

(25) Minceva-Sukarova, B.; Sherman, W. F.; Wilkinson, G. R. The Raman Spectra of Ice (Ih, II, III, V, VI and IX) as Functions of Pressure and Temperature. *J. Phys. C: Solid State Phys.* **1984**, *17*, 5833–5850.

(26) Fanetti, S.; Falsini, N.; Bartolini, P.; Citroni, M.; Lapini, A.; Taschin, A.; Bini, R. Superheating and Homogeneous Melting Dynamics of Bulk Ice. *J. Phys. Chem. Lett.* **2019**, *10*, 4517–4522.

- (27) Vatamanu, J.; Kusalik, P. G. Observation of Two-Step Nucleation in Methane Hydrates. *Phys. Chem. Chem. Phys.* **2010**, *12*, 15065–15072.
- (28) Liang, S.; Kusalik, P. G. Exploring Nucleation of H₂S Hydrates. *Chem. Sci.* **2011**, *2*, 1286–1292.
- (29) He, Z.; Linga, P.; Jiang, J. What are the Key Factors Governing the Nucleation of CO₂ Hydrate? *Phys. Chem. Chem. Phys.* **2017**, *19*, 15657–15661.
- (30) Jin, Y.; Nagao, J.; Hayashi, J.; Shimada, W.; Ebinuma, T.; Narita, H. Observation of Xe Hydrate Growth at Gas-Ice Interface by Microfocus X-ray Computed Tomography. *J. Phys. Chem. C* **2008**, *112*, 17253–17256.
- (31) Moudrakovski, I. L.; Sanchez, A. A.; Ratcliffe, C. I.; Ripmeester, J. A. Nucleation and Growth of Hydrates on Ice Surfaces: New Insights from ¹²⁹Xe NMR Experiments with Hyperpolarized Xenon. *J. Phys. Chem. B* **2001**, *105*, 12338–12347.
- (32) Uchida, T.; Takeya, S.; Wilson, L.; Tulk, C.; Ripmeester, J.; Nagao, J.; Ebinuma, T.; Narita, H. Measurements of Physical Properties of Gas Hydrates and in Situ Observations of Formation and Decomposition Processes via Raman Spectroscopy and X-Ray Diffraction. *Can. J. Phys.* **2003**, *81*, 351–357.
- (33) Ohmura, R.; Ogawa, M.; Yasuoka, K.; Mori, Y. H. Statistical Study of Clathrate-Hydrate Nucleation in a Water/Hydrochlorofluorocarbon System: Search for the Nature of the “Memory Effect”. *J. Phys. Chem. B* **2003**, *107*, 5289–5293.
- (34) Buchanan, P.; Soper, A. K.; Thompson, H.; Westacott, R. E.; Creek, J. L.; Hobson, G.; Koh, C. A. Search for Memory Effects in Methane Hydrate: Structure of Water Before Hydrate Formation and After Hydrate Decomposition. *J. Chem. Phys.* **2005**, *123*, 164507.
- (35) Shi, L.; Ni, Y.; Drews, S. E. P.; Skinner, J. L. Dielectric Constant and Low-Frequency Infrared Spectra for Liquid Water and Ice Ih within the E3B Model. *J. Chem. Phys.* **2014**, *141*, 084508.
- (36) Citroni, M.; Fanetti, S.; Falsini, N.; Foggi, P.; Bini, R. Melting Dynamics of Ice in the Mesoscopic Regime. *Proc. Natl. Acad. Sci. U. S. A.* **2017**, *114*, 5935–5940.